# Layered charge-density waves with nanoscale coherence in $YBa_2Cu_3O_{7-\delta}$

Makoto Maki*
*Department of Physics, Saga University, Saga 840-8502, Japan*

Terukazu Nishizaki, Kenji Shibata,† and Norio Kobayashi
*Institute for Materials Research, Tohoku University, Sendai 980-8577, Japan*
(Received 4 April 2005; published 22 July 2005)

We have used a scanning tunneling microscope to investigate the electronic state of CuO chains in $YBa_2Cu_3O_{7-\delta}$. The observed one-dimensional charge modulations form the nanoscale coherent domains, exhibiting an existence of the interchain correlations. For Zn-substituted crystal, the influence of the local destruction of planar superconductivity is not seen. These results are explained in terms of the very short-range charge-density waves formed in a monolayer with the atomic vacancies.

DOI: 10.1103/PhysRevB.72.024536 PACS number(s): 74.72.Bk, 68.37.Ef, 74.50.+r

## I. INTRODUCTION

Low-dimensional materials have drawn a lot of attraction since they exhibit a variety of characteristic condensed states at low temperatures. One of the most fundamental states is a charge density wave (CDW) stemmed from the particular topology of Fermi surface. In one-dimensional (1D) electronic systems, a considerable divergence of 1D electron response function $\chi(\mathbf{q})$ occurs at $|\mathbf{q}|=2k_F$, where $k_F$ is the Fermi wave number. This innate $2k_F$ instability comes out through the Fermi-surface nesting in real quasi-1D or two-dimensional (2D) materials and combines with the lattice distortion with $2k_F$ periodicity, resulting in $2k_F$-CDW formation. Low-temperature scanning tunneling microscopy (LT-STM) has proven to be a very useful technique for investigating the CDW states, because it can visualize the spatial distributions of charge densities directly at an atomic scale. Since the pioneering work by Coleman *et al.*,[1] the most successful scanning tunneling misroscopy (STM) investigation of CDW states have been done for a family of transition-metal dichalcogenides such as $1T$-$TaS_2$, $1T$-$TaSe_2$, or $2H$-$NbSe_2$. These materials are 2D-CDW systems, showing the CDW- superlattice images well below the corresponding CDW-transition temperatures. In contrast to 2D CDW, STM observation for a 1D CDW is limited in number and one of the precious examples have been reported on transition-metal trichalcogenides such as $NbSe_3$.[2,3] The CDW states with three-dimensional long-range order are regarded as the *bulk*-CDW systems. Recently, LT-STM studies also demonstrate that the *surface* of some semiconductors and metals exhibits 1D- or 2D-CDW transitions.[4–8] These results indicate that even a limited number of electrons in the surface bands can lead to a symmetry-breaking charge rearrangement to lower the total energy of corresponding part of the material.

Similar charge-density ordering has been observed via LT-STM measurements on $YBa_2Cu_3O_{7-\delta}$ (YBCO), one of the most famous high-temperature superconductors (HTSC).[9–14] On the exposed 1D CuO-chain layers of cold-cleaved YBCO, there appears to be 1D charge-density corrugations with a period of $\sim$1.3 nm along the $b$ axis. Since HTSC materials are composed of several different atomic layers whose electronic structures are different from each other, only a small fraction of electrons in the CuO-chain band may concern an occurrence of the electronic density modulations, such as surface CDWs. In case of YBCO, however, three characteristics complicate the situation. First, HTSCs are regarded as the strongly correlated materials. Highly correlated 1D electronic system is known to have the large quantum fluctuations, bringing about the breakdown of the Fermi-liquid states. Second, the CuO-chain layers have a number of oxygen vacancies that form clusters along the chains.[12] It is well known that even a few impurities or point defects locally perturb the phase coherence of the bulk-CDW order,[15,16] and more crucial role of such imperfections has been reported on the surface-CDW formation.[17,18] The last one is that there probably exists the superconducting condensate on the CuO chains, though its origin is still unclear.[19,20] The energy-resolved charge-density modulations reported through recent scanning tunneling spectroscopy (STS) measurement are considered as the spatial oscillations of resonance states in terms of the superconducting quasi-particles scattering.[14,21]

In our previous paper,[13] we have presented the oxygen-content dependence of charge-modulation wavelengths on the CuO-chain layer, which is in favor of the $2k_F$-CDW scenario originated in the quasi-1D Fermi surface nesting. However, the observed charge periodicity seem to remain in phase over a few hundred angstroms along the CuO-chain direction (i.e., the $b$ direction) and over a still shorter distance in the $a$ direction; that is still an open question. If we accept the $2k_F$-CDW scenario, our result should indicate the loss of the CDW long-range order, bringing about a further question of how the CDW state sets in the chain layer of YBCO.

In order to solve these questions and to elucidate the electronic structure of the CuO chains, we have proceeded with LT-STM investigations of YBCO single crystals with various oxygen contents and with a small amount of Zn impurities. We have paid attention to the following two points: (1) How the interchain correlations reside in the charge-density modulations, and (2) how the local destruction of superconductivity in the $CuO_2$ plane affects the electronic state of chains.

 

Our present studies strongly suggest that the short-range CDW order is stabilized in connection with the pinning potential related to a cluster of oxygen vacancies. We can also interpret this short-range CDW order as the anisotropically attenuated CDW, that is, the 1D Friedel oscillations with the finite interchain correlations. The CuO-chain images of Zn-doped YBCO are quite similar to those of Zn-free one, indicating that the planar superconductivity does not exert influence on the CDW state of the CuO chains.

## II. EXPERIMENT

The experiments were carried out in a commercial ultrahigh vacuum (UHV) LT-STM (UNISOKU Co., Ltd.) upon which we made some improvements ourselves.[22] All STM images shown here were taken at 4.5 K using the mechanically sharpened Pt-Ir tips. Single crystals of YBCO were grown by a self-flux method using yttria crucibles and annealed under 1 bar oxygen at various temperatures to obtain the target oxygen content.[23] Superconducting transition temperatures $T_c$ were determined by magnetization measurements using a SQUID magnetmeter, showing 89, 92, 78, and 59 K for highly overdoped ($\delta \simeq 0.02$), slightly overdoped ($\delta \simeq 0.06$), underdoped ($\delta \simeq 0.20$), and heavily underdoped ($\delta \simeq 0.35$) concentrations, respectively. $YBa_2(Cu_{0.997}Zn_{0.003})_3O_{7-\delta}$ single crystal was prepared by the same method. The actual Zn concentration was determined by inductively coupled plasma spectrometry and the homogeneous Zn distribution was confirmed with electron-probe microanalysis. The oxygen content was controlled by the same annealing condition for slightly overdoped Zn-free YBCO ($\delta \simeq 0.06$), resulting in a $T_c \simeq 88$ K with a transition width of $\sim$1.5 K. Since YBCO has a highly reactive surface that is easily degraded in the UHV environment above $\sim$40 K, all samples were mechanically cleaved *in situ* below 20 K immediately before the LT-STM measurements. The *ab*-surface termination of cleaved YBCO is known to be composed of BaO and CuO-chain layers.[12] In this paper, we show the LT-STM images obtained only on the latter layers.

## III. RESULTS

### A. Interchain correlations

Figure 1 shows a constant-height STM image of CuO chains in underdoped YBCO with a $T_c$ of $\simeq$78 K. The electronic corrugations with 1D character, the direction of which are assigned to the *b* axis, are clearly seen. The distance between the neighboring charge alignments is estimated to be $\sim$3.9 Å, which coincides with the lattice constant of YBCO. Along the *b* axis, the wavelength $\lambda_b$ of the observed corrugations is approximately 1.12 nm. As briefly discussed in our previous letter,[13] the value of $\lambda_b$ becomes shorter with decreasing the oxygen content $7-\delta$, and this phenomenon is well understood by considering the $2k_F$ instability in 1D CuO chains. Charge alignments shown in Fig. 1 contain a few (about one out of three alignments) depressions due to the nearly 20% oxygen deficiencies. Unfortunately, it is difficult to discuss the oxygen arrangement quantitatively, since the atomic images without any modulations have not been

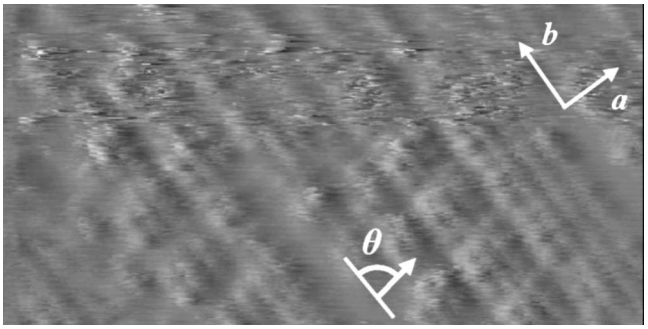


FIG. 1. Constant-height image (55 Å$\times$110 Å) of the CuO-chain layer in underdoped YBCO ($T_c \simeq 78$ K), taken with $V_{\text{sample}} = -150$ mV and $I = 0.45$ nA.

obtained on the oxygen-reduced CuO-chain layers. A very noticeable aspect of the charge arrangement in Fig. 1 is that several 1D corrugations partitioned by the depression are placed at a constant angle. Those *in-phase* regions are regarded as atomic-scale ordered domains and strongly suggest the existence of interchain correlations. In order to characterize the direction of the interchain correlation, we introduce an angle $\theta$ between a line connecting the center of neighboring bright (or dark) images and the *b* axis, as illustrated within Fig. 1. The definition of $\theta$ signifies a periodic charge arrangement perpendicular to the chain direction, i.e., 1D charge corrugations spaced $\lambda_a = \lambda_b \tan\theta$ apart along the *a* axis are in phase. The value of $\theta$ for underdoped YBCO is $\sim$80° from Fig. 1.

Figures 2(a)–2(d) respectively show four kinds of CuO-chain images for highly overdoped, slightly overdoped, underdoped, and heavily underdoped YBCO. All images are 55 Å$\times$110 Å, and the oxygen-content dependence of $T_c$ is also shown schematically. The charge arrangement tends to lose its fine structures with increasing oxygen vacancy $\delta$: The chains in highly overdoped YBCO are relatively uniform in intensity and have the smallest number of depressions, whereas on underdoped samples the regular pattern of the charge modulation is broken here and there. The best-ordered charge distribution is found in the middle part of Fig. 2(a), enclosed by a parallelogram. It is natural to consider this well-correlated pattern as the intrinsic charge ordering, since it is hardly influenced by the oxygen vacancies in this area. In the 90 K crystals shown in Figs. 2(a) and 2(b), the correlation lengths of the charge corrugations are estimated to be a few hundred angstroms along the *b* axis and only a few lattice constants along the *a* axis, which is consistent with those of a previous LT- STM/STS study.[14] Although it is difficult to strictly define a unique $\theta$-value in each figure, the values obtained in relatively well-ordered areas are $\sim$40° and $\sim$55° for highly overdoped [Fig. 2(a)] and slightly overdoped YBCO [Fig. 2(b)], respectively. In 80 K YBCO shown in Fig. 2(c), the charge correlation obviously exists between the oxygen-vacant lines, and the still larger $\theta$-value of $\sim$80° is obtained as mentioned above. The electronic corrugations still maintain the 1D character for a further oxygen-reduced sample, as can be seen in Fig. 2(d) of the 60 K crystal, whereas the *a*-directional correlation has been lost and each charge alignment is almost independent. We

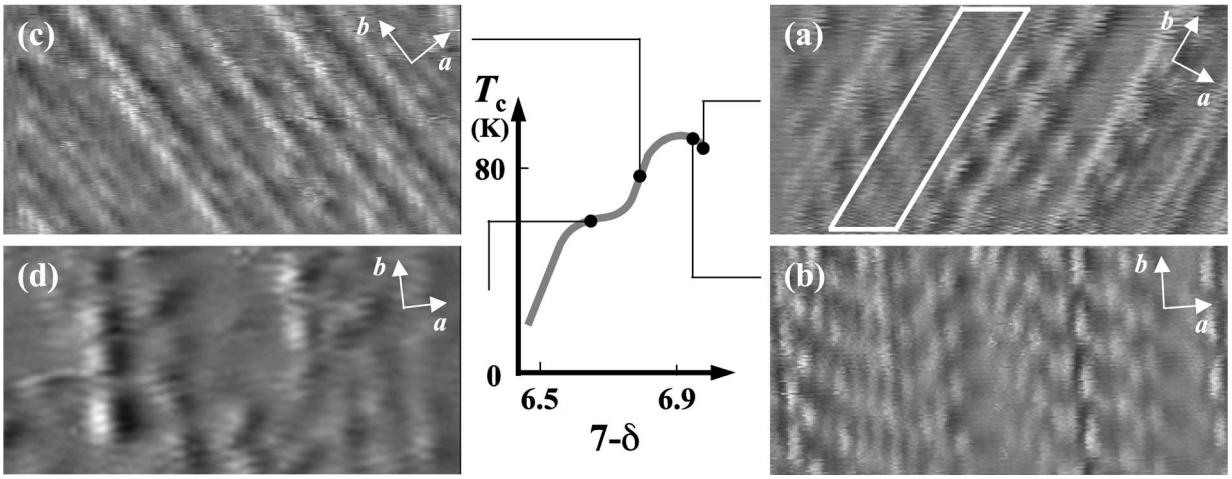


FIG. 2. Four kinds of CuO-chain constant-height images for (a) highly overdoped, (b) slightly overdoped, (c) underdoped, and (d) heavily underdoped YBCO. All images are 55 Å × 110 Å. Tunneling conditions are (a) $V_{\text{sample}}=-10$ mV, $I=0.45$ nA, (b) $V_{\text{sample}}=-20$ mV, $I=0.45$ nA, (c) $V_{\text{sample}}=-300$ mV, $I=0.50$ nA, (d) $V_{\text{sample}}=-300$ mV, $I=0.45$ nA.

emphasize that the formation of the correlated domains is reduced by the oxygen-vacant lines but the 1D character in the charge arrangement is essentially maintained in the heavily underdoped samples. This observation suggests that the inherent charge-density ordering has 1D-electronic nature and is significantly affected by the oxygen vacancies, resulting in the highly anisotropic and surprisingly short correlated regions.

### B. Zn-substitution effect

Zn substitution for planar Cu is well known to have a strong effect on HTSC. Pan *et al.*[24] performed LT-STM/STS measurements around Zn impurities in $Bi_2Sr_2CaCu_2O_{8+\delta}$ (Bi2212) crystals and presented the quasi-particle scattering resonances in good agreement with the so-called Swiss-cheese model for the local suppression of superconductivity.[25] Also in YBCO, the substituted Zn atoms locate primarily at the planar Cu sites and radically suppress $T_c$. In order to elucidate the relationship between the observed charge-density ordering and the superfluid component resident in the crystal, therefore, we have investigated how the local destruction of planar superconductivity affects the electronic modulations in chains.

A constant-height image and a constant-current (topographic) image of the same CuO-chain area in Zn-doped YBCO are shown in Figs. 3(a) and 3(b), respectively. The observed 1D modulations have a wavelength $\lambda_b$ of $\sim$1.3 nm, which is in good agreement with the value of the slightly overdoped Zn-free sample. As reported previously, on the BaO layer, very striking electronic patterns induced by Zn substitution have been observed on the low-bias voltage measurements.[26] Conversely, on the CuO-chain images, there is no noticeable difference between samples with and without Zn impurities, though the individual chains are hardly distinguishable due to the strong interchain correlations.

Now, we summarize the characteristics of the CuO-chain STM-images, all of which are also recognized on Zn-doped crystals. The charge corrugations are known to be more prominent as the applied bias voltage is lowered, and on the higher-bias measurements several 1D depressions tend to appear instead.[9,27] From a sequence of seven images shown in Fig. 4, it is evident that the chain images of Zn-YBCO have the same tendency, which is independent of the bias polarity. During a tip scanning, the atomic resolution occasionally undergoes a sudden change and a different pattern comes into view, probably due to the subtle change of tunneling conditions.[10,12] Figure 5 taken on Zn-substituted YBCO shows the similar change; consequently, the high-resolution chain-images come out in the lower middle part. When the bias polarity is reversed, it has been reported that the phase of charge corrugation is delayed by $\pi$.[10] Since even a slight thermal drift, if it exists, would prevent the exact identification of an atomic site, it is difficult to detect the phase shift without any landmarks, such as defects or impurities. Fortunately, in the lower left-hand corner of Fig. 6, there is a dark area with a few weak bumps which probably correspond to the underlying crystalline defects. Judging from the phase difference relative to this fixed standard, we know that the reversed-bias corrugation image has an opposite sign for Zn-YBCO. Hence, it follows that slight Zn impurities do not

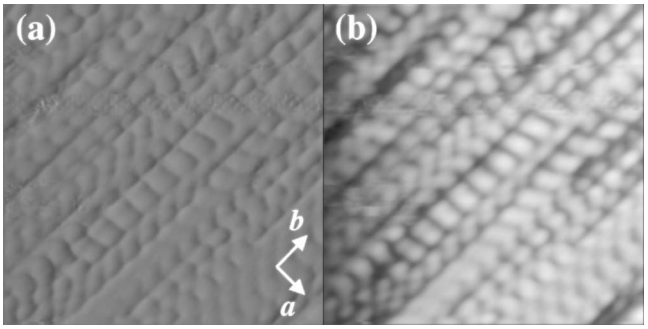


FIG. 3. (a) Constant-height image and (b) constant-current (topographic) image taken on the same area (160 Å on a side) of CuO-chain layer in 0.3%-Zn-doped YBCO ($T_c \simeq 88$ K). $V_{\text{sample}}=50$ mV and $I=0.10$ nA.

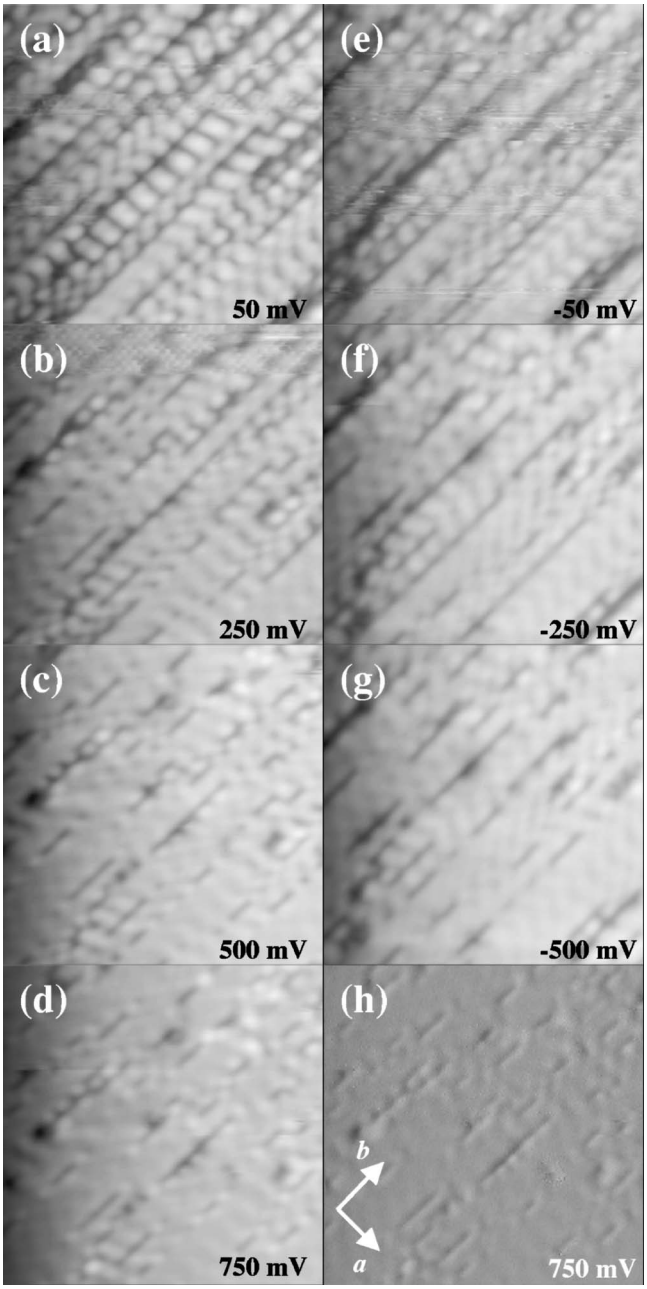


FIG. 4. Sequence of seven constant-current (topographic) images (160 Å on a side) in 0.3%-Zn-doped YBCO at a series of sample bias voltage: (a) 50 mV, (b) 250 mV, (c) 500 mV, (d) 750 mV, (e) −50 mV, (f) −250 mV, and (g) −500 mV ($I$ =0.10 nA). (h) Constant-height image taken under the same tunneling condition for (d).

have any effects on the CuO-chain properties, which is in contrast with the considerable influence on the $CuO_2$ plane.

## IV. DISCUSSION

The primary observation of our experiments is that the adjacent chain images are arranged *in phase* at a certain angle with the $b$ direction. Especially for 80 K sample, we can easily find that those correlations are blocked by the

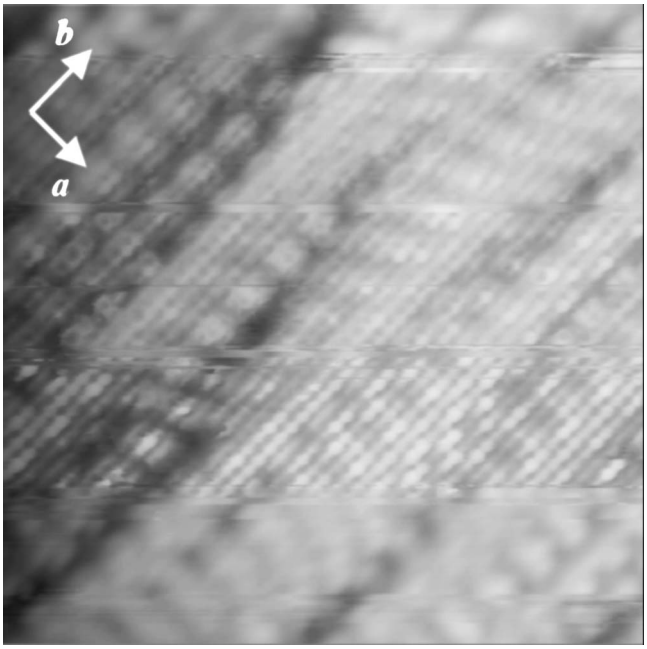


FIG. 5. Topographic image (160 Å on a side) in 0.3%-Zn-doped YBCO, taken with $V_{\text{sample}}$=50 mV and $I$=0.10 nA.

oxygen-vacant lines or die off abruptly, resulting in the *nanoscale coherent domains*. From a different point of view, it also seems that the oxygen defects stabilize a location of the in-phase region, but their arrangement destroys the long-range coherence. In this section, the observed charge modulation is discussed in terms of the interplay between the inherent charge-density ordering and the random lattice potential associated with the oxygen defects.

As shown in Fig. 2, the correlation direction denoted by $\theta$ systematically changes with oxygen vacancies. This result suggests that the intrinsic charge-density ordering is closely related to the hole concentration and very sensitive to the Fermi-surface topology. The charge-corrugation images on CuO chains are schematically represented in Fig. 7(a). Here, we introduce a vector $\vec{\lambda}$ whose components are $\lambda_a(=\lambda_b \tan\theta)$ and $\lambda_b$. The corresponding wave-vector $\vec{Q}$ denotes the nesting direction in **k** space is illustrated by Fig.

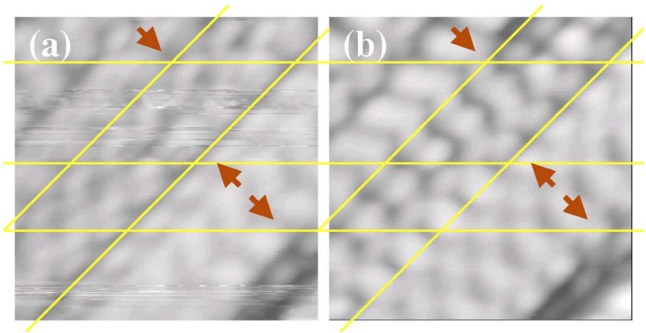


FIG. 6. (Color online). (a) Filled-state ($V_{\text{sample}}$=−50 mV) and (b) empty-state ($V_{\text{sample}}$=50 mV) topographic images in 0.3%-Zn-doped YBCO (80 Å on a side, $I$=0.10 nA). 180° out of phase images are clearly seen at the points marked with arrows.

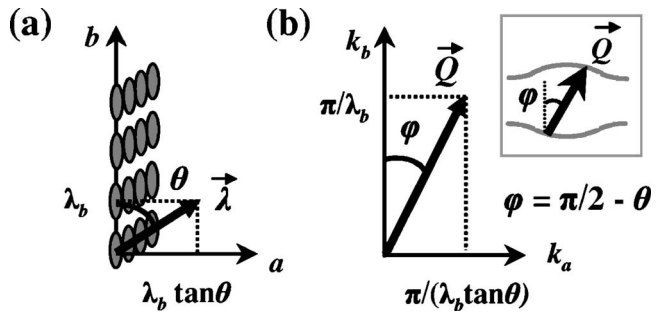


FIG. 7. (a) Schematic drawing of charge-density alignments in the CuO-chain layer. $\vec{\lambda}$ denotes a direction of the interchain correlation. (b) Corresponding nesting-vector $\vec{Q}$ in **k** space. Inset: Schematic drawing of Fermi-surface nesting in the CuO-chain layer.

7(b). Our experiments show that the nesting angle $\varphi$ between $\vec{Q}$ and the $k_b$ axis monotonically decreases with decreasing hole concentration. When a finite transfer integral perpendicular to the chain direction is present, the Fermi surface is distorted and the nesting direction is shifted as illustrated in the inset of Fig. 7(b). Hence, the observed charge arrangement can be naturally understood as a $2k_F$ CDW originating from the quasi-1D Fermi-surface nesting with finite interchain correlations, leaving the Coulomb repulsion out of consideration.

To interpret the possible stabilization of the very-short-range CDW, it is necessary to consider the interaction between CDW correlations and lattice imperfections. In the general picture of CDW formation, the fluctuating amplitude begins to develop well above a three-dimensional CDW-transition temperature $T_{3D}$.[28] By decreasing the temperature to $T_{3D}$, the 1D correlations along the chains are gradually extended and the interchain correlations—which are much shorter than the chain-directional ones—also grow up. Below $T_{3D}$, the fluctuations on the neighboring chains couple, leading to the long-range CDW-state. In our case of YBCO, concerning the existence of oxygen vacancies, the observed nanoscale coherent domains can be regarded as the underdeveloped CDW fluctuations pinned by the lattice through the interaction with them. Note that an oxygen vacancy may act as a charged defect and also bring about the local lattice distortion.[23] Thus, we can understand the reason why the nesting angles $\varphi$ are scattered within the same sample, whereas the corrugation wavelengths $\lambda_b$ can be decided in connection with the oxygen content.

It is important to mention that the formation of pinned CDW domains has been also seen in artificial metal surfaces with defects or foreign adsorbates.[17,18,29] In both of the two cases, the CDW condensate is very sensitive to the extrinsic defects, and stabilization with its coherence remains incomplete. A common background is that the $2k_F$ instability resides in a monolayer (or just a few atomic layers in the case of surfaces). We consider that these *CDW sheets* are apt to be divided into the coherent domains, because of their imperfect interlayer coupling. Then, in case of quasi-1D systems, such as CuO chains, considerably anisotropic domains come into existence. Interestingly, also on the impurity-doped 1D *bulk*-CDW system, Ti- and Ta-$NbSe_3$, the anisotropic CDW domains have been reported via x-ray scattering experiments.[30]

The CDW fluctuations pinned by impurities can be also regarded as the CDW structures coupled with Friedel oscillations around the impurity sites. Because of the same wave number of $2k_F$, a strong interaction or competition between CDW and Friedel oscillation is expected to take place locally at an atomic scale. Tüttő and Zawadowski[31] have pointed out that if Friedel oscillations around the weak impurities are out of phase relative to CDW, a pair of bound states appears in the energy-gap spectrum. Recent LT-STS results[14] indicating that the resonance peaks in the CuO-chains spectra seems consistent with their suggestion. It is reasonable that a dispersive charge-density oscillation is observed in the local density of states (LDOS) maps which reflect the *energy-resolved* values of the charge-density distribution.[14] On the other hand, LT-STM provides the energy- integrated LDOS, which is dominated by a *cutoff* wave number $k_F$ due to the discontinuity at the Fermi level. In the CuO-chain layer, the oxygen-vacancy cluster is a strong candidate for the scattering source. Anyway, an existence of oxygen defects is considered to be essential for the formation of the short-range CDW patches with no mobility.

Finally, we would like to mention the relationship between the CuO-chain CDW and the planar superconductivity. As shown in Fig. 3(b), there is no clear Zn-substitution effect upon the CuO-chain images. This experimental result strongly suggests that almost all of the Zn impurities occupy the planar Cu sites and the chain layers are not disturbed directly by them. A more noticeable aspect is that the Zn impurities which reside in the $CuO_2$ plane also have hardly any effect on the chain images: The resonance peak at the Zn site or the local suppression of superconductivity over a coherence length around it, both of which have been observed on Bi2212,[24] cannot be detected through the chain's CDW. Our observations indicate that the charge modulation is not the work of the proximity-superconducting quasi-particles, and imply very little correlation between the chain's CDW and the superconducting condensate in the plane. On the other hand, to interpret the anisotropy of superfluid density found in the *ab* plane,[19] the chain layer is supposed to have the additional condensate. Though one possible explanation is that the nanoscale CDW and the superconductivity occur in separate sections of the same Fermi surface, the anisotropic suppression of the condensate density brought by Zn doping is still unsolved.[32] We have now set about further LT-STM and STS studies for YBCO with various Zn or Ni densities in order to elucidate the chain-plane coupling.

## V. SUMMARY

The $2k_F$ CDW originated in the Fermi-surface topology has been visualized on the CuO-chain layer in cold-cleaved YBCO. The chain CDW is essentially 1D and the interchain correlations are also seen. The observed charge-density modulations form the very short-range in-phase domains, which are well understood considering the CDW-defect interactions. We cannot find a remarkable difference in CDW images between Zn-doped and Zn-free samples, indicating that the superconducting quasi-particles have nothing to do with the CDW formation.

**ACKNOWLEDGMENTS**

This work was performed under the Interuniversity Cooperative Research Program of the Institute for Materials Research, Tohoku University, and partially supported by a research project, Grant-in-Aid for Scientific Research (B) (15340107) by the Ministry of Education, Sports, Science, and Technology of Japan.

*Electronic address: mmaki@cc.saga-u.ac.jp

†Present address: Institute of Industrial Science, The University of Tokyo, 4-6-1 Komaba, Meguro-ku, Tokyo 153-8505, Japan.

[1] R. V. Coleman, B. Drake, P. K. Hansma, and G. Slough, Phys. Rev. Lett. **55**, 394 (1985).

[2] C. G. Slough, B. Giambattista, A. Johnson, W. W. McNairy, and R. V. Coleman, Phys. Rev. B **39**, R5496 (1989).

[3] Zhenxi Dai, C. G. Slough and R. V. Coleman, Phys. Rev. Lett. **66**, 1318 (1991).

[4] J. M. Carpinelli, H. H. Weitering, E. W. Plummer, and R. Stumpf, Nature (London) **381**, 398 (1996).

[5] J. M. Carpinelli, H. H. Weitering, M. Bartkowiak, R. Stumpf, and E. W. Plummer, Phys. Rev. Lett. **79**, 2859 (1997).

[6] H. W. Yeom, S. Takeda, E. Rotenberg, I. Matsuda, K. Horikoshi, J. Schaefer, C. M. Lee, S. D. Kevan, T. Ohta, T. Nagao, and S. Hasegawa, Phys. Rev. Lett. **82**, 4898 (1999).

[7] T. Nakagawa, G. I. Boishin, H. Fujioka, H. W. Yeom, I. Matsuda, N. Takagi, M. Nishijima, and T. Aruga, Phys. Rev. Lett. **86**, 854 (2001).

[8] K. Swamy, A. Menzel, R. Beer, and E. Bertel, Phys. Rev. Lett. **86**, 1299 (2001).

[9] H. L. Edwards, J. T. Markert, and A. L. de Lozanne, Phys. Rev. Lett. **69**, 2967 (1992).

[10] H. L. Edwards, A. L. Barr, J. T. Markert, and A. L. de Lozanne, Phys. Rev. Lett. **73**, 1154 (1994).

[11] H. L. Edwards, D. J. Derro, A. L. Barr, J. T. Markert, and A. L. de Lozanne, Phys. Rev. Lett. **75**, 1387 (1995).

[12] M. Maki, T. Nishizaki, K. Shibata, and N. Kobayashi, J. Phys. Soc. Jpn. **70**, 1877 (2001).

[13] M. Maki, T. Nishizaki, K. Shibata, and N. Kobayashi, Phys. Rev. B **65**, 140511(R) (2002).

[14] D. J. Derro, E. W. Hudson, K. M. Lang, S. H. Pan, J. C. Davis, J. T. Markert, and A. L. de Lozanne, Phys. Rev. Lett. **88**, 097002 (2002).

[15] B. Giambattista, A. Johnson, R. V. Coleman, B. Drake, and P. K. Hansma, Phys. Rev. B **37**, R2741 (1988).

[16] X. L. Wu and C. M. Lieber, Phys. Rev. B **41**, R1239 (1990).

[17] H. H. Weitering, J. M. Carpinelli, A. V. Melechko, J. Zhang, M. Bartkowiak, and E. W. Plummer, Science **285**, 2107 (1999).

[18] A. V. Melechko, J. Braun, H. H. Weitering, and E. W. Plummer, Phys. Rev. Lett. **83**, 999 (1999).

[19] D. N. Basov, R. Liang, D. A. Bonn, W. N. Hardy, B. Dabrowski, M. Quijada, D. B. Tanner, J. P. Rice, D. M. Ginsberg, and T. Timusk, Phys. Rev. Lett. **74**, 598 (1995).

[20] R. Gagnon, S. Pu, B. Ellman, and L. Taillefer, Phys. Rev. Lett. **78**, 1976 (1997).

[21] D. K. Morr and A. V. Balatsky, Phys. Rev. Lett. **90**, 067005 (2003).

[22] M. Maki, T. Nishizaki, K. Shibata, T. Sasaki, and N. Kobayashi, Physica C **357**, 291 (2001).

[23] T. Nishizaki, K. Shibata, T. Naito, M. Maki, and N. Kobayashi, J. Low Temp. Phys. **117**, 1375 (1999).

[24] S. H. Pan, E. W. Hudson, K. M. Lang, H. Eisaki, S. Uchida, and J. C. Davis, Nature (London) **403**, 746 (2000).

[25] B. Nachumi, A. Keren, K. Kojima, M. Larkin, G. M. Luke, J. Merrin, O. Tchernyshöv, Y. J. Uemura, N. Ichikawa, M. Goto, and S. Uchida, Phys. Rev. Lett. **77**, 5421 (1996).

[26] M. Maki, T. Nishizaki, and N. Kobayashi, Phys. Rev. B **67**, 014534 (2003).

[27] M. Maki, T. Nishizaki, K. Shibata, and N. Kobayashi, Physica C **378**, 84 (2002).

[28] G. Grüner, *Density Waves in Solids* first edition, (Addison-Wesley, Reading, MA, 1994).

[29] S. S. Lee, J. R. Ahn, N. D. Kim, J. H. Min, C. G. Hwang, J. W. Chung, H. W. Yeom, Serguei V. Ryjkov, and S. Hasegawa, Phys. Rev. Lett. **88**, 196401 (2002).

[30] S. Rouzière, S. Ravy, J.-P. Pouglet, and R. E. Thorne, Phys. Rev. B **59**, 15121 (1999).

[31] I. Tüttő and A. Zawadowski, Phys. Rev. B **32**, 2449 (1985).

[32] N. L. Wang, S. Tajima, A. I. Rykov, and K. Tomimoto, Phys. Rev. B **57**, R11081 (1998).